

Simulation of 2D Cavitation Bubble Growth Under Shear Flow by Lattice Boltzmann Model

Xiaopeng Chen^{1,2,*}

¹ School of Mechanics, Civil Engineering and Architecture, Northwestern Polytechnical University, Xi'an, Shaanxi 710072, China.

² Multidisciplinary Research Group for Virtual and Real Environment, Northwestern Polytechnical University, Xi'an, Shaanxi 710072, China.

Received 8 January 2009; Accepted (in revised version) 11 May 2009

Communicated by Yao Zheng

Available online 4 August 2009

Abstract. Natural cavitation is defined as the phenomenon of the formation of vapor bubbles in a flow due to the pressure falls below the liquid's vapor pressure. The inception of the cavitation bubble is influenced by many factors, such as impurities, turbulence, liquid thermal properties etc. In this paper, we simulate a 2D cavitation "bubble" growth under shear flow in the inception stage by Single-Component-Multiphase Lattice Boltzmann Model (SCMP LBM). An empirical boundary condition sensitive 2D bubble growth rate, $R \sim e^f$, is postulated. Furthermore, the comparison is conducted for bubble behavior under different shear rates. The results show that the cavitation bubble deformation is coincident with prior droplet theories and the bubble growth decreases slightly with the flow shear rate.

AMS subject classifications: 76T10, 76M28, 65Z05

Key words: Bubble dynamics, cavitation, lattice Boltzmann methods, Rayleigh-Plesset equation.

1 Introduction

Natural cavitation is defined as the phenomenon of the formation of vapor bubbles in a flow due to the pressure falls below the liquid's vapor pressure, which can cause the falling of fluid machinery performance [1, 2], or drag reducing for high speed underwater vehicles [3]. In the past decades, numerous efforts were contributed to the cavitation bubble inception [4, 5], which can be treated as the initial condition for the bubble evolution. However, the study shows that the cavitation inception is more complex than we

*Corresponding author. Email address: xchen76@nwpu.edu.cn (X. P. Chen)

described at the beginning of this paragraph. It is influenced by the number and qualities of the nuclei in the liquids, the flow structure, thermodynamic parameters etc. And different inception forms were found, including bubble band, bubble ring, traveling bubble, traveling patch, fixed patch, and developed attached cavitation [4].

In addition to the experimental and scaling analyses, numerical simulation is conducted widely as a powerful tool for the cavitation study. Coupling with the thermodynamic models Vortmann et al. [6] applied the volume of fluid method to predict typical effects of cavitations. By finite volume method, Chau et al. [7] studied the hydrodynamic characters of foils. Particular emphasis was placed by Kunz et al. [8] on solve two-phase Reynolds Averaged Navier-Stokes equations (RANS), which included prediction strategy, flux evaluation, limiting strategies etc. The capabilities of the method were further validated through a comparison between axisymmetric and 3D RANS simulations by the same group [9]. Senocak and Shyy [10] applied a pressure-velocity-density coupling scheme to handle the large density ratio cavitating flow. Seo et al. [11] proposed a density-based homogeneous equilibrium model with a linearly-combined EOS to predict cavitating flow noise. To capture the acoustic waves in two-phase flow, the central compact finite difference scheme was implemented. Lu et al. [3] compared different cavitation models numerically. Ventilated and natural cavitation flows were studied. Besides the class of surface capture methodologies, as mentioned above, surface tracking methods were applied as well, where the interfaces are treated as time dependent boundaries of computational domain [12].

For the traditional partial differential equation based numerical simulation, two major obstacles should be combatted. The first one is the numerical scheme. Since across the interface, phase properties, such as density and viscosity, vary steeply, the numerical schemes should be designed carefully to prevent the nonphysical oscillations. Limiting strategies, filtering techniques or sophisticated interface updating algorithms should be applied. Secondly, the phase transition model should be postulated correctly according to the thermodynamic fundamentals.

In recent decades, lattice Boltzmann methods (LBM) emerged as an attractive CFD method, which bases on the mesoscale particle dynamics [13–15]. Some sophisticated flow phenomena, such as interfacial flow, reactive flow, are simulated successfully by combined with certain particle properties, whose motion is simply divided into "collision" and "stream" loops. Shan and Chen [16] postulated a long range interaction, by which the liquid phase transition and interfacial tension were simulated perfectly. Swift [17] coupled Cahn-Hilliard free energy formula with LBM, where phase separation and two-phase flow modeling were validated to be feasible. The key issue of the two models is to reproduce the non-ideal gas EOS. Later on, multiphase LBM were applied in many fields [18–21]. Yuan and Schaefer [22] compared different EOS with Chen-Shan's model. Sukop [23] validated the capability of LBM to simulate the cavitation problems by Shan-Chen's model. 2D bubble evolution (growth or collapse) were reported.

In this paper, our first goal is to demonstrate the feasibility of LBM on cavitation simulation further. With LBM, we also intend to study the 2D cavitation bubble growth

under shear flow during its inception stage, which is of lack for traditional numerical simulations. The **scientific definition** of inception is adopted in our work, "*...the initial rapid growth of vapor- and gas-filled bubbles as a consequence of hydrodynamic forces.*" [4]. It should be noted that, in published SCMP LBM models, both vapor and liquid phase share the common relaxation time, which leads to the same viscosity [21]. Albeit it could lead some errors, the simulation results in quiescent liquid agree with Rayleigh-Plesset model well. In the situation of shear flow, the results are compared with the quiescent case to analyze the shear flow influences.

The paper is organized as following. In Section 2, the LBM method coupled with Shan-Chen's multiphase model is introduced briefly. The flow domain setup is described in this section as well. In Section 3, the bubble growth under quiescent and shear flow are analyzed, which are compared with Rayleigh-Plesset and other bubble dynamic models respectively. Conclusions are drawn in Section 4.

2 Numerical models

2.1 SCMP lattice Boltzmann model

A crucial idea of lattice Boltzmann model is, both the location and velocity of the particles, which compose the fluids, are discretized (see Fig. 1). The typical LB equation is presented as,

$$f_i(\mathbf{x} + \mathbf{e}_i \Delta t, t + \Delta t) - f_i(\mathbf{x}, t) = -\frac{1}{\tau} \cdot (f_i(\mathbf{x}, t) - f_i^{eq}(\mathbf{x}, t)), \quad i=0,1,\dots,b, \quad (2.1)$$

where f_i denotes the particle velocity distribution function along the i th direction, f_i^{eq} the corresponding local equilibrium distribution satisfying Maxwell distribution. \mathbf{x} , \mathbf{e}_i ($i=0,1,\dots,b$) are the lattice site coordinates and the particle velocities towards the nearest-neighboring sites respectively. b is the number of the neighbors. The lattice Boltzmann equation implies two kinds of particle motions, streaming and collision. On the LHS of Eq. (2.1), particles jump from local site, \mathbf{x} , to its nearest-neighboring sites, $\mathbf{x} + \mathbf{e}_i \Delta t$, on each time step, $\Delta t \equiv 1$. On the RHS, the collision leads loss or gain of the particles with velocity of \mathbf{e}_i . On the other hand, after collision, the velocity distribution will relax to equilibrium distribution, f_i^{eq} .

In this study, D2Q9 model is applied, which is depicted in Fig. 1. The equilibrium velocity distribution reads,

$$f_i^{eq}(x, t) = w_i \rho(x) \left[1 + 3 \frac{\mathbf{e}_i \cdot \mathbf{u}}{c^2} + \frac{9}{2} \frac{(\mathbf{e}_i \cdot \mathbf{u})^2}{c^4} - \frac{3}{2} \frac{u^2}{c^2} \right], \quad (2.2)$$

where the weights w_i are 4/9 for the rest particles ($i=0$), 1/9 for $i=1,2,3,4$, and 1/36 for $i=5,6,7,8$ (as in Fig. 1). \mathbf{u} , c are macro-velocity and the lattice speed. The corresponding

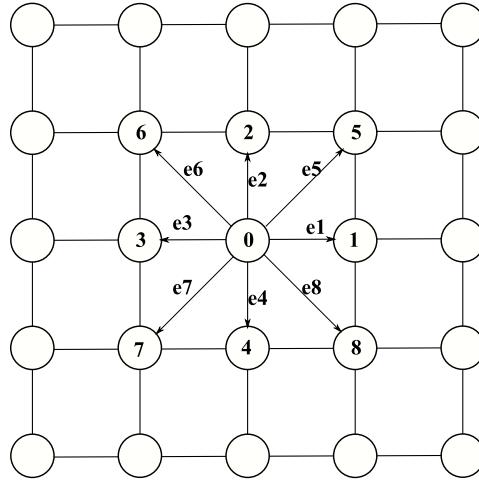


Figure 1: Schematic diagram for D2Q9 model.

macro-variables are defined as,

$$\rho = \sum_{i=0}^8 f_i, \quad (2.3)$$

$$\rho \mathbf{u} = \sum_{i=0}^8 (f_i \cdot \mathbf{e}_i), \quad (2.4)$$

$$\mu = (2\tau - 1) / 6. \quad (2.5)$$

For typical LBM, the ideal gas equation of state is satisfied, $P = \rho/3$.

Following Shan and Chen's model [16], long range interactions between fluid particles, or non-ideal gas effects, are applied in our work, which influence the averaged velocity, \mathbf{u} , in Eq. (2.2). The forces actually lead to the phase separation, for both single- and multi-components, if it's large enough [24]. In our D2Q9 model, it is given by,

$$\mathbf{F} = -\mathcal{G}\psi((x), t) \sum_{i=1}^8 w_i \psi(\mathbf{x} + \mathbf{e}_i \Delta t, t) \mathbf{e}_i, \quad (2.6)$$

where \mathcal{G} is the interaction strength, with $\mathcal{G} < 0$ representing attractive forces. And ψ is the effective density, namely,

$$\psi(\rho) = \psi_0 \exp(-\rho_0 / \rho), \quad (2.7)$$

following Sukop's work [23]. In the equation, ψ_0 and ρ_0 are the arbitrary constants. Therefore, after a collision, we have the modified net momentum,

$$\rho \mathbf{u} = \sum_{i=1}^8 f_i \cdot \mathbf{e}_i + \tau \mathbf{F}. \quad (2.8)$$

The simplified pressure is obtained after correlating Eq. (2.1) with the Navier-Stokes equations by Chapman-Enskog expansion [16],

$$P = \frac{\rho}{3} + \frac{\mathcal{G}}{6} [\psi(\rho)^2] \quad (2.9)$$

which is not an ideal gas EOS. At the critical point, both first- and second-order pressure derivatives with respect to the density are zero, i.e.,

$$(\partial P / \partial v)_T = (\partial^2 P / \partial v^2)_T = 0.$$

The critical value of \mathcal{G}_c can be obtained. For $\mathcal{G} < \mathcal{G}_c$, at a single pressure, two densities of the same material can coexist, namely, phase separation. The interfacial tension, which stems from inter-molecular forces, could be evaluated simply through the pressure difference of a circular interface.

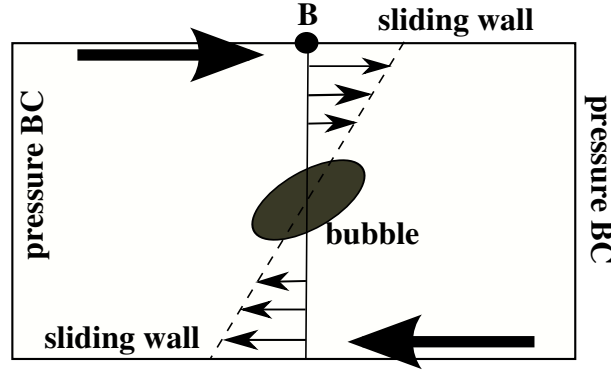


Figure 2: Computational domain.

2.2 Computational domain

In this work, the computational domain, 500×400 , is set as shown in Fig. 2. The upper- and down-side boundaries are imposed with constant velocity, which have same values but opposite directions ($v_B = \pm 0.02, \pm 0.05, \pm 0.08, \pm 0.1$). Zou-He's boundary condition model is applied [25] on these two sides. Left- and right-side boundaries are imposed with constant density/pressure. The value of the boundary density is set following Sukop's procedure [26]. For a certain fluid, phase densities are computed in the flat-interface liquid-vapor system. The density boundary condition is then set with the values a little lower than the liquids in the flat interface case. In this study, Sukop's [23] parameters are adopted, $\rho_0 = 200$, $\psi_0 = 4.0$, $\mathcal{G} = -120$, while $\tau = 1.0$. Our flat interface results show the liquid density $\rho_L = 524.2$ and vapor density $\rho_v = 85.7$. The density on the sides is $\rho_{Bound} = 500$, accordingly.

With these parameters, the bubble will collapse if the initial size is smaller than $R_{crt} = 6$ due to the large interfacial tension. To catch the shear flow influence on the bubble

growth, $R_{ini} = 8$ is chosen. The initial density condition is set $\rho_{in} = 80$ inside the bubble and $\rho_{out} = \rho_{Bound} = 500$ outside the bubble. The velocity is initialized with fully developed shear flow profile (as in Fig. 2), and the velocity distribution function, f_i , is calculated through Eq. (2.2).

3 Results and analysis

3.1 Bubble growth in quiescent domain

The bubble growth in quiescent liquid is calculated as benchmark, and the results are to be compared with the shear flow cases. In this section, the simulation is implemented with two domain size, 300×300 and 500×400 respectively. The purpose is to check the domains size influences, as discussed below.

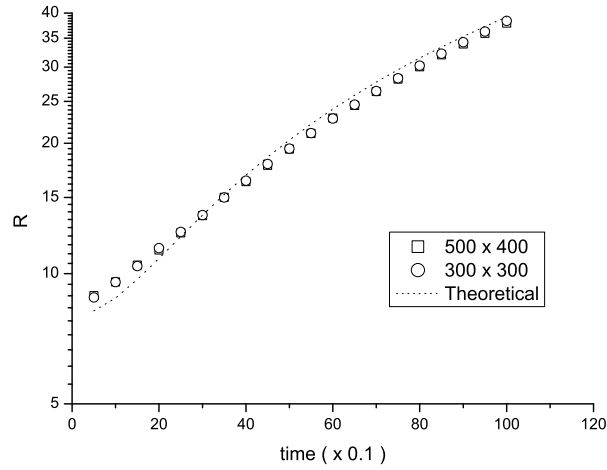


Figure 3: Bubble growth in rest liquid, \square : 500×400 , \circ : 300×300 , \cdots : Runge-Kutta simulation.

The bubble radius revolution is plotted in Fig. 3. The behavior of a single bubble in an infinite domain of liquid at rest far from the bubble and with uniform temperature far from the bubble can be described by Rayleigh-Plesset equation [1], namely,

$$\frac{p_B(t) - p_\infty(t)}{\rho_L} = R \frac{d^2 R}{dt^2} + \frac{3}{2} \left(\frac{dR}{dt} \right)^2 + \frac{4\nu_L}{R} \frac{dR}{dt} + \frac{2S}{\rho_L R}, \quad (3.1)$$

where ρ represents density, the subscripts B , L , ∞ the bubble, liquid and infinity respectively. R is the bubble radius, and S interfacial tension. p is pressure. In our case, the domain is 2D, and therefore the equation is modified as following.

The symbols are defined as same as in chapter 2 of Brennen's textbook [1]. In the liquid, the conservation of mass requires that,

$$u_r(r, t) = \frac{F(t)}{r}, \quad (3.2)$$

where $F(t)$ is related to $R(t)$ by a kinematic boundary condition at the bubble surface. And at bubble surface, we also have $u(R,t) = dR/dt$. Therefore,

$$F(t) = R \frac{dR}{dt}. \quad (3.3)$$

In cylindrical coordinate, Navier-Stokes equation for motion in the r direction,

$$\frac{\partial u_r}{\partial r} + u_r \frac{\partial u_r}{\partial r} = -\frac{1}{\rho_L} \frac{\partial p}{\partial r} + \dots. \quad (3.4)$$

Substituting Eq. (3.2) into Eq. (3.4) and integrating the resulting equation from R to r_∞ , we obtain

$$\ln\left(\frac{r_\infty}{R}\right) \cdot \frac{dF}{dt} - \frac{F^2(t)}{2r^2} = \frac{p - p_\infty}{\rho_L}, \quad (3.5)$$

which implies, in 2D situations, the bubble growth is boundary condition sensitive. Furthermore, a pressure boundary condition on the bubble surface can be achieved,

$$\left(-p - \frac{2\mu_L}{\rho_L R} \frac{dR}{dt} + p_B - \frac{S}{R}\right) \Big|_{r=R} = 0. \quad (3.6)$$

Substituting Eqs. (3.3) and (3.6) into Eq. (3.5) yields,

$$\ln\left(\frac{r_\infty}{R}\right) \cdot (\dot{R}^2 + R\ddot{R}) - \frac{\dot{R}^2}{2} + \frac{2\mu_L}{\rho_L R} \dot{R} - \frac{S}{\rho_L R} = \frac{p_B - p_\infty}{\rho_L}. \quad (3.7)$$

In our simulations, the far field boundary varies from $10R \sim 16R$, corresponding to

$$\ln\left(\frac{r_\infty}{R}\right) = 2.3 \sim 2.8,$$

during $t = 0 \sim 700$. Hence, the $\ln\frac{r_\infty}{R}$ could be treated as piecewise constants approximately. Runge-Kutta method is applied to solve Eq. (3.7) numerically with $\ln\left(\frac{r_\infty}{R}\right) \equiv 2.5$. Other parameters are calculated through Eq. (2.3) to Eq. (2.9). And the result is plotted in Fig. 3, which agrees well with the LBM simulations. The largest deviation occurs at the beginning stage (less than 10%), which may be caused by the unprecise initial density condition, when the interface density profile relaxation couples with the bubble growth.

Furthermore, we discuss the following equation which keeps the terms of high orders of Eq. (3.7),

$$\ddot{R}^2 + R\ddot{R} + \frac{\dot{R}}{R} = 0, \quad (3.8)$$

which yields $\ln R \propto t$. Through Fig. 3, the computational results fit the relation $\ln R \propto t$ quite well. In Fig. 3, the results with different domain size are compared, where only slightly discrepancy is found at around $t = 1000$.

At last, it should be pointed out that, in Rayleigh-Plesset model ρ_v/ρ_L is sufficiently small, while in our case it is close to 0.16. Further study should be implemented in the future.

3.2 Bubble growth under shear flow

The nonspherical cavitation bubble inception plays important roles in the wake cavitation, where high shear rate flow couples with vortex evolution. Moreover, bubble deformation in a second immiscible liquid is full of scientific and technical values [27]. In this section, we focus on the bubble growth in pure shear flow.

As described in Section 2, the cavitation bubble is undergone a shear flow with the shear rate

$$G = \frac{v_B}{h} \propto v_B,$$

where h is the gap size between the upper and down walls. A typical bubble growth sequence is shown in Fig. 4.

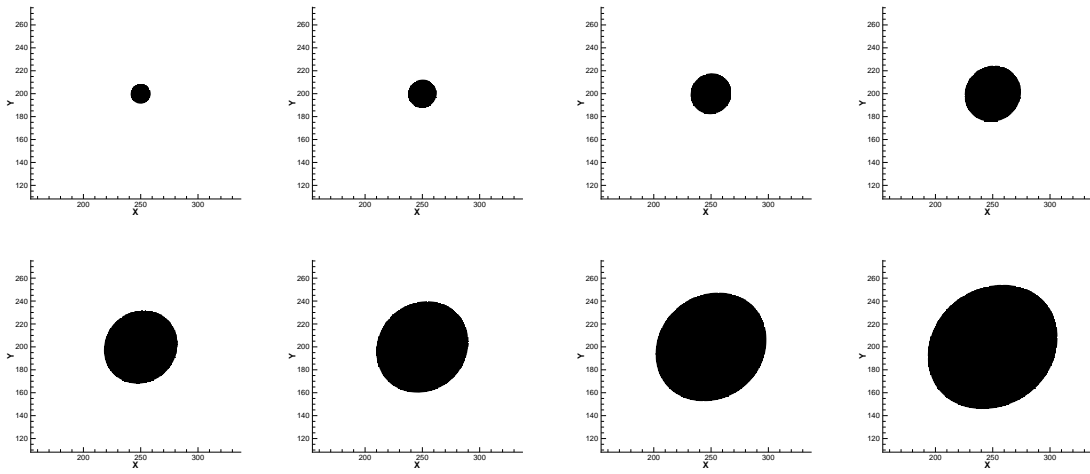


Figure 4: Bubble deformation in shear flow with $G=0.05$. The interval between each subfigure is 200 steps.

Two parameters may be worthy to be compared, i.e., the deformation and growth rate. Here, the vapor and liquid interface is defined as $\rho = 297.1$, which equals to $(\rho_v + \rho_L)/2$, $t = 50$. Following Rallison [27], we define a dimensionless deformation D by

$$D = (l - b) / (l + b), \quad (3.9)$$

where l and b are the largest and smallest distance from the bubble center to the interface, respectively. The deformation for all sliding velocities and time instants are plotted in Fig. 5, where $Ca = \mu Ga / S$ is the capillary number, which denotes the ratio of shear force to the interfacial tension. Both of the characteristic viscosity μ and the interfacial tension S are set as 1, since they keep constant for all cases. And a is set as l . The linear relationship between Ca and D implies that, in the inception stage, the viscous and interfacial tension effects predominate the bubble deformation, which is the characters of small size scale flow [27]. In Fig. 5, the fitting line does not pass the origin of the coordinate, which is led by the initial phase densities relaxation, and the discrepancy can be ignored.

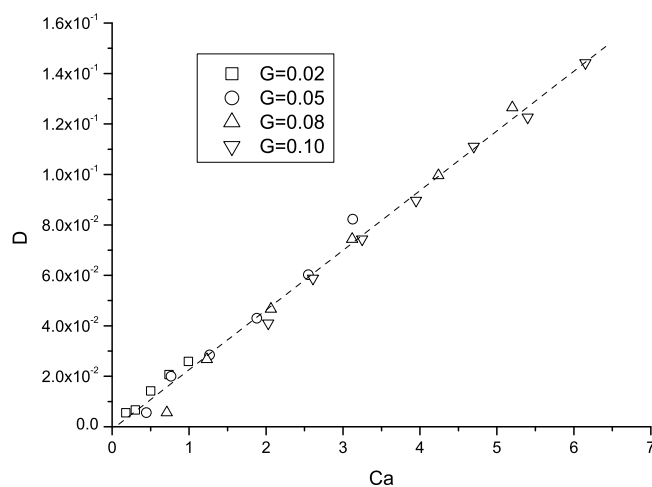


Figure 5: The relationship between deformation D and capillary number Ca .

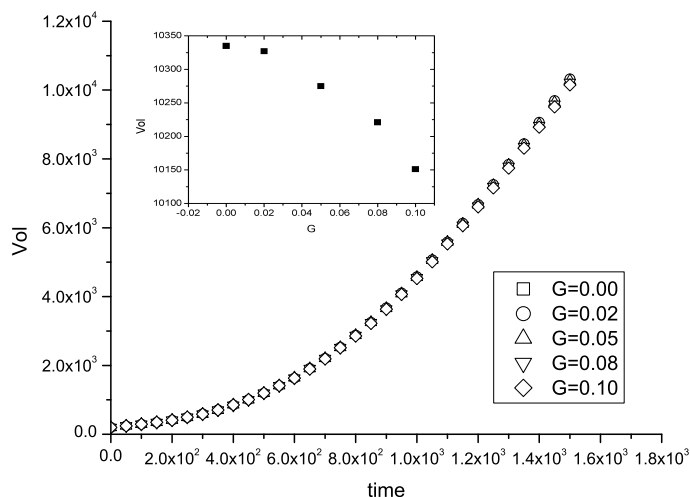


Figure 6: Bubble growth in shear flow. Inset: bubble volume at $t=1500$.

In Fig. 6, the volume (Vol , the area for $\rho < 297.1$) evolution is compared under different shear rates. The results show little, but nonzero, discrepancy among the different G (as in the inset of Fig. 6). It is interesting to compare the details among the cases, as in Table 1, where the subscript C denotes the bubble center and $mass = \rho_C \times Vol$. In Fig. 7, the pressure distribution inside the bubbles at $t=1500$ is depicted. It is observed that the shear flow rises the bubble pressure. This can not be due to the bubble size variety purely, since the mean interface curvature ($\propto \sqrt{Vol}$) of the bubble varies by 1% from $G=0.0$ to $G=0.1$, while that of the pressure varies only by 0.1%. It contradicts the results in Section

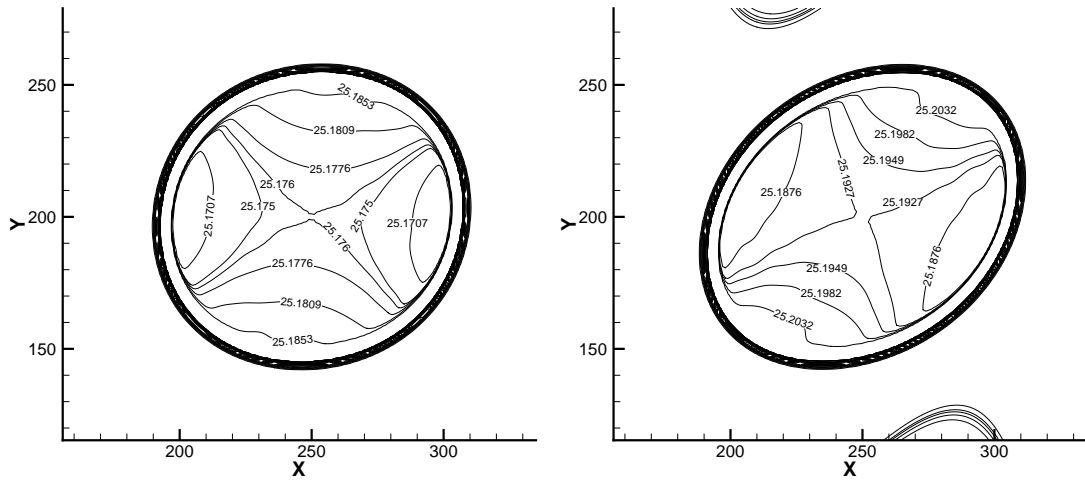


Figure 7: Bubble pressure distribution for $G=0.02$ (left) and $G=0.08$ (right), $t=1500$.

Table 1: Data comparison for $t=1500$.

G	ρ_C	p_C	$mass$
0.00	83.50	25.174	862972
0.02	83.51	25.176	862408
0.05	83.54	25.182	858373
0.08	83.60	25.192	854476
0.10	83.66	25.203	849233

3.1, namely, the bubble growth is driven by the bubble pressure.

Two possible reasons may lead to the above phenomenon: (i) One is the numerical errors, *either* inherent, such as semi-incompressibility, vanishing Mach number assumption, *or* errors during post-processes, such as the identify of interface (the flow condition causes the variety of equilibrium phase density, and thus the real interface location); (ii) another one, as mentioned at the end of Section 3.1, is that the density ratio between vapor and liquid is large, and mass rate of evaporation, or the mass flow of liquid inward, should not be ignored (as in [1]). The higher bubble pressure will decelerate the rate of phase transition and thus the growth rate.

4 Conclusions and discussions

In this paper, we simulate the cavitation bubble growth in rest and in shear flows with Shan-Chen's SCMP lattice Boltzmann model. The feasibility of the model is validated. The conclusions can be drawn as:

- In quiescent environment, cavitation bubble grows with $\ln R \propto t$ approximately, which is in agreement with deduced 2D Rayleigh-Plesset model. Different to 3D Rayleigh-Plesset model, the bubble growth is boundary condition sensitive in 2D.

- In shear flow, the bubble will be stretched and the deformation $D \propto Ca$, which is coincident with normal bubble dynamics. By increasing the shear rate, the bubble growth rate will slightly decrease. The possible reason may be due to the numerical errors or the high ρ_v/ρ_L ratio.

According to our results, the following aspects can be improved in the further study, although the lattice Boltzmann methods can be used to capture many cavitation phenomena:

- The ρ_v/ρ_L should be decreased further by applying a better multiphase LB model;
- Variable viscosities should be set differently to vapor and liquid phases in simulations for practical purposes;
- Larger shear rate can be applied to obtain a larger bubble deformation to get a more clear picture of the shear rates influences during bubble inception. In this work, the v_B is set with the limitation of $Ma \ll 1$;
- For real cavitation flow, thermal effects, bubble-bubble and bubble-solid interactions, bubble-vortex interaction all play important roles. These effects should be considered as well.

Acknowledgments

The author would like to thank Professor C.W. Zhong, Professor J.S. Jiang at NWPU, and Professor J.J. Feng at UBC for their helpful discussions on the relevant scientific and technical issues. The author would like to thank the support of University Foundation for Fundamental Research of NWPU.

References

- [1] C.E. Brennen, *Cavitation and Bubble Dynamics*, Oxford University Press, New York, 1995.
- [2] R.E.A. Arndt, Cavitation in fluid machinery and hydraulic structures, *Ann. Rev. Fluid Mech.*, 13(1981), 273-328.
- [3] C.J. Lu, Y.S. He, X. Chen et al., Numerical and experimental research on cavitating flows, *New trends in fluid mechanics research*, 5th International conference on fluid mechanics, Tshinghua Univ. Press, Beijing, 2007.
- [4] E.P. Rood, Review-Mechanics of cavitation inception, *J. Fluids Engineering*, 113(1991), 163-175.
- [5] R.E.A. Arndt, Cavitation vortical flows, *Ann. Rev. Fluid Mech.*, 34(2002), 143-175.
- [6] C. Vortmann, G.H. Schnerr, S. Seelecke, Thermodynamic modeling and simulation of cavitating nozzle flow, *Heat and Fluid Flow*, 24(2003), 774-783.
- [7] S.W. Chau, K.L. Hsu, J.S. Kouh et al., Investigation of cavitation inception characteristics of hydrofoil sections via a viscous approach, *Marine Science and Technology*, 8(2004), 147-158.

- [8] R.F. Kunz, D.A. Boger, D.R. Stinebring, et al., A preconditioned Navier-Stokes method for two-phase flows with application to cavitation prediction, *Computers and Fluids*, 29 (2000), 849-875.
- [9] J.W. Lindau, R.F. Kunz, D.A. Boger, et. al., High reynolds number unsteady, multiphase CFD modeling of cavitating flows, *J. Fluids Engineering*, 124(2002), 607-616.
- [10] I. Senocak, W. Shyy, A pressure-based method for turbulent caviating flow computations, *J Compt. Phys*, 176(2002), 363-383.
- [11] J.H. Seo, Y.J. Moon and B.R. Shin, Prediction of cavitating flow noise by direct numerical simulation, *J Comput. Phys*, 227(2008), 6511-6531.
- [12] L.J. Liu, J. Li, Z.P. Feng, A numerical method for simulation of attached cavitation flows, *Int'l J. Numerical Methods Fluids*, 52(2006), 639-658.
- [13] S. Succi, *The Lattice Boltzmann Equation for Fluid Dynamics and Beyond*, Oxford Univ. Press, New York, 2001.
- [14] D.A. Wolf-Gladrow, *Lattice-Gas Cellular Automata and Lattice Boltzmann Models*, Springer-Verlag, Berlin, 2000.
- [15] S. Chen, G.D. Doolen, Lattice Boltzmann method for fluid flows, *Ann. Rev. Fluid Mech.*, 30(1998), 329-364.
- [16] X.W. Shan, H.D. Chen, Lattice Boltzmann model for simulating flows with multiple phases and components, *Phys. Rev. E.*, 47(1993), 1815-1819.
- [17] M.R. Swift, W.R. Osborn and J.M. Yeomans, Lattice boltzmann simulation of nonideal fluids, *Phys. Rev. E*, 75(1995), 830-834.
- [18] M.M. Dupin, I. Halliday and C.M. Care, Multi-component lattice boltzmann equation fo mesoscale blood flow, *J. Physics A: Mathematical and General*, 36(2003), 8517-8534.
- [19] W.F. Huang, Y. Li and Q.S. Liu, Application of the lattice Boltzmann method to electrohydrodynamics: deformation and instability of liquid drops in electrostatic fields, *Chinese Science Bulletin*, 52(2007), 3319-3324.
- [20] J.M. Buick, J.A. Cosgrove and R. Higham, Acoustic lattice Boltzmann model for immiscible binary fluids with a species-dependent impedance, *Phys. Rev. E*, 76(2007), 036713.
- [21] A. Tentner, H. Chen, R. Zhang, Simulation of two-phase flow and heat transfer phenomena in a boiling water reactor using the lattice Boltzmann method, *Physica A*, 362(2006), 98-104.
- [22] P. Yuan, L Schaefer, Equations of state in lattice Boltzmann model, *Phys. Fluids*, 18(2006), 042101.
- [23] M.C. Sukop, D. Or, Lattice Boltzmann method for homogeneous and heterogeneous cavitation, *Phys. Rev. E*, 71(2005), 046703.
- [24] J.S. Rowlinson, B. Widom, *Molecular Theory of Capillarity*, Oxford Press, New York, 1982.
- [25] Q. Zou, X. He, On pressure and velocity boundary conditions for the lattice Boltzmann BGK model, *Phys. Fluids*, 9(1997), 1591-1598.
- [26] M.C. Sukop, D.T. Thorne Jr., *Lattice Boltzmann Modeling*, Springer-Verlag, Berlin Heidelberg, 2007.
- [27] J.M. Rallison, The deformation of small viscous drops and bubbles in shear flows, *Ann. Rev. Fluid Mech.*, 16(1984), 45-66.